Compromised Mitochondrial Protein Import Acts as a Signal for UPR^mt

Graphical Abstract

Highlights

- Impairment of most, but not all, mitochondrial processes causes UPR^mt

- Conditions inducing UPR^mt lead to a decrease in mitochondrial membrane potential

- Decrease in mitochondrial membrane potential acts as a signal that triggers UPR^mt

- The MTS of ATFS-1 acts as a sensor for decreased mitochondrial membrane potential

Authors

Stéphane G. Rolland, Sandra Schneid, Melanie Schwarz, ..., Dejana Mokranjac, Eric Lambie, Barbara Conradt

Correspondence

rolland@bio.lmu.de (S.G.R.),
b.conradt@ucl.ac.uk (B.C.)

In Brief

Unfolded protein stress is proposed to be the signal that triggers UPR^mt. Rolland et al. propose instead that a decrease in mitochondrial membrane potential acts as a signal. Furthermore, they show that the MTS of the transcription factor ATFS-1 is essential to sense this signal and activate UPR^mt.
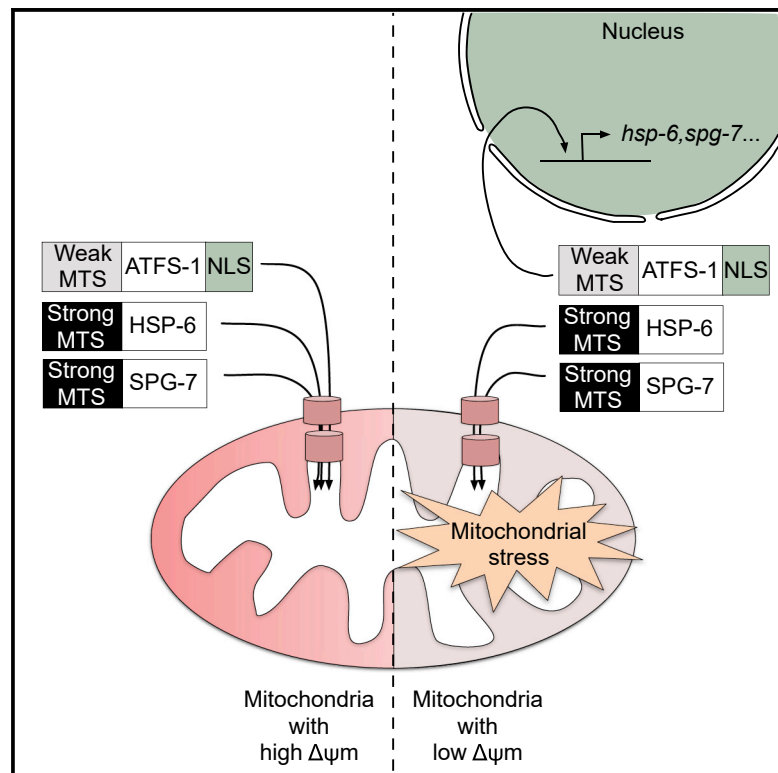
CellPress

Report

Compromised Mitochondrial Protein Import Acts as a Signal for UPRmt

Stéphane G. Rolland,[1,*] Sandra Schneid,[1] Melanie Schwarz,[1] Elisabeth Rackles,[1] Christian Fischer,[1,2] Simon Haeussler,[1] Saroj G. Regmi,[1,6] Assa Yeroslaviz,[3] Bianca Habermann,[3,5] Dejana Mokranjac,[4] Eric Lambie,[1,7] and Barbara Conradt[1,2,7,8,*]

[1]Faculty of Biology, LMU Munich, 82152 Planegg-Martinsried, Germany
[2]Center for Integrated Protein Science, LMU Munich, 82152 Planegg-Martinsried, Germany
[3]Max Planck Institute of Biochemistry, Computational Systems Biochemistry, Am Klopferspitz 18, 82152 Martinsried, Germany
[4]Biomedical Center Munich – Physiological Chemistry, LMU Munich, 82152 Planegg-Martinsried, Germany
[5]Present address: Aix-Marseille University, CNRS, IBDM UMR 7288, 13009 Marseille, France
[6]Present address: Division of Molecular and Cellular Biology, National Institute of Child Health and Human Development, NIH, Bethesda, MD 20892, USA
[7]Present address: Department of Cell and Developmental Biology, University College London, London, UK
[8]Lead Contact
*Correspondence: rolland@bio.lmu.de (S.G.R.), b.conradt@ucl.ac.uk (B.C.)
https://doi.org/10.1016/j.celrep.2019.07.049

SUMMARY

The induction of the mitochondrial unfolded protein response (UPRmt) results in increased transcription of the gene encoding the mitochondrial chaperone HSP70. We systematically screened the *C. elegans* genome and identified 171 genes that, when knocked down, induce the expression of an *hsp-6* HSP70 reporter and encode mitochondrial proteins. These genes represent many, but not all, mitochondrial processes (e.g., mitochondrial calcium homeostasis and mitophagy are not represented). Knockdown of these genes leads to reduced mitochondrial membrane potential and, hence, decreased protein import into mitochondria. In addition, it induces UPRmt in a manner that is dependent on ATFS-1 but that is not antagonized by the kinase GCN-2. We propose that compromised mitochondrial protein import signals the induction of UPRmt and that the mitochondrial targeting sequence of ATFS-1 functions as a sensor for this signal.

INTRODUCTION

Ensuring that proteins acquire and maintain their proper conformation is essential, as unfolded or misfolded proteins are inactive and can form toxic aggregates that lead to disease (Macario et al., 2005). Protein quality control occurs at all times but can be upregulated via the "unfolded protein response" (UPR). UPR occurs in multiple cellular compartments, allowing localized responses to specific stresses (Gardner et al., 2013; Jovaisaite et al., 2014; Vabulas et al., 2010).

Mitochondrial UPR (UPRmt) has been best characterized in the nematode *Caenorhabditis elegans*. The UPRmt transcription factor ATFS-1 contains both mitochondrial and nuclear localization sequences (Nargund et al., 2012). In the absence of mitochondrial stress, ATFS-1 is imported into mitochondria and degraded by the mitochondrial protease LONP-1 (Nargund et al., 2012). Under stress conditions, unfolded proteins in the mitochondrial matrix have been proposed to be cleaved into peptides by the protease CLPP-1 (Haynes et al., 2007, 2010). Peptides generated are thought to be exported across the inner mitochondrial membrane (IMM) by the ABC transporter HAF-1 (Haynes et al., 2010). The release of peptides through HAF-1 has been proposed to block mitochondrial import by an unknown mechanism, resulting in the relocalization of ATFS-1 to the nucleus, where it activates the transcription of genes encoding mitochondrial chaperones and proteases (Haynes et al., 2010; Nargund et al., 2012). This pathway is at least partially conserved in mammals (Fiorese et al., 2016; Yano, 2017). An additional pathway has been described in *C. elegans*, which involves the cytoplasmic kinase GCN-2 (Baker et al., 2012). GCN-2 has been proposed to be activated by ROS generated by dysfunctional mitochondria. Once activated, GCN-2 phosphorylates the translation initiation factor eIF2α, thereby blocking general cytosolic translation, which has been proposed to help regain mitochondrial proteostasis by reducing the protein folding load of mitochondrial chaperones (Baker et al., 2012). Hence, the induction of UPRmt is antagonized by the kinase GCN-2.

In *C. elegans*, UPRmt can be induced by different types of stress, such as the knockdown of nuclear genes encoding subunits of the electron transport chain (ETC) (Durieux et al., 2011) or a block in mitochondrial translation (Houtkooper et al., 2013). These perturbations alter the stoichiometry between mitochondria- and nuclear-encoded ETC subunits ("mito-nuclear imbalance"), leading to the accumulation of unassembled subunits of ETC complexes and causing unfolded protein stress (Houtkooper et al., 2013). This stress has been proposed to trigger UPRmt (Yoneda et al., 2004), but the mechanism through which this signal is transduced to the nucleus remains unclear.

To systematically identify genes and processes that trigger UPRmt when compromised, we performed a genome-wide RNAi screen in *C. elegans*. We found that impairment of most,
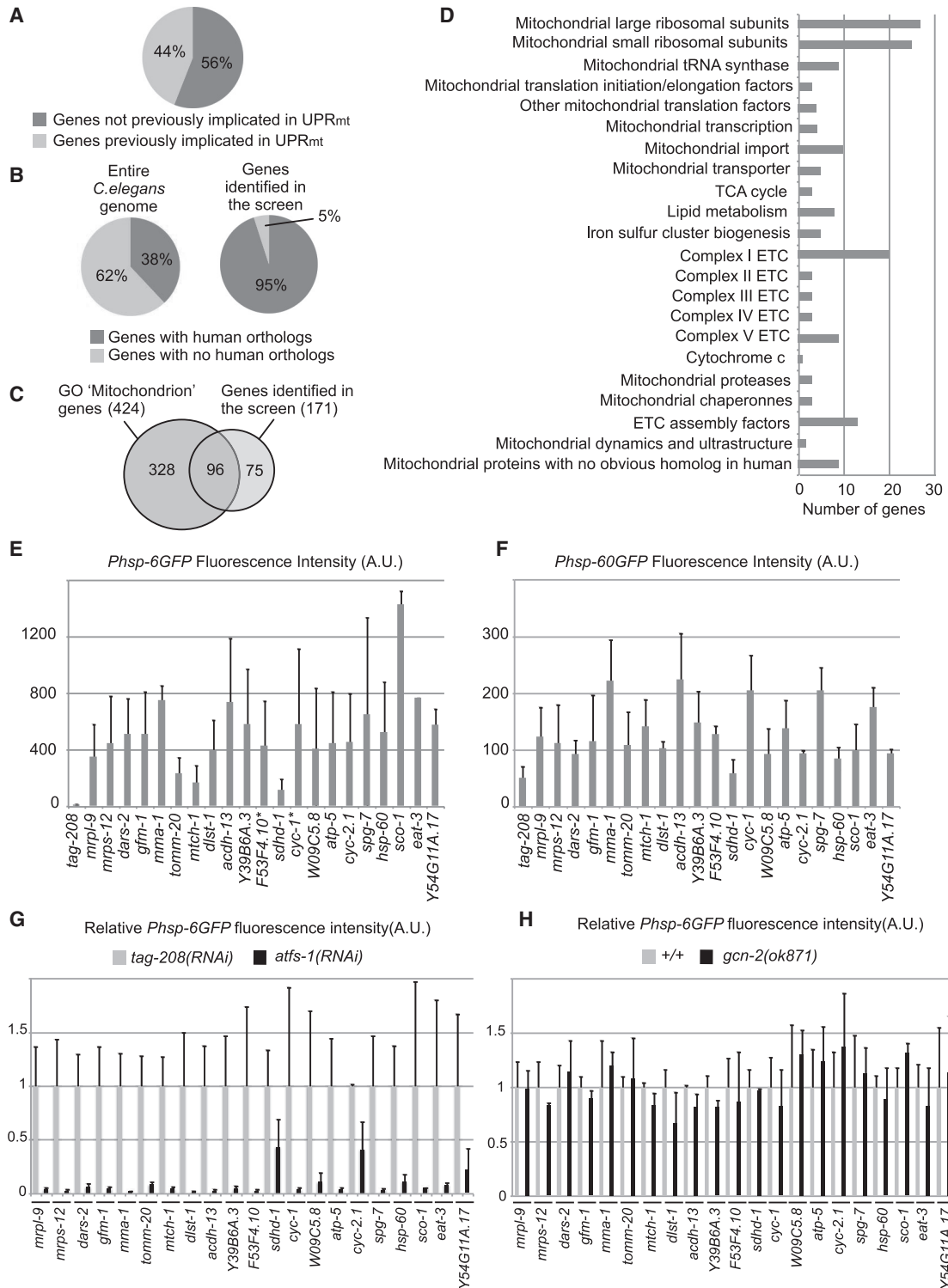
A

44% | 56%

■ Genes not previously implicated in UPRmt
■ Genes previously implicated in UPRmt

B

Entire *C.elegans* genome — Genes identified in the screen

62% | 38%   5% | 95%

■ Genes with human orthologs
■ Genes with no human orthologs

C

GO 'Mitochondrion' genes (424)   Genes identified in the screen (171)

328 | 96 | 75

D

Mitochondrial large ribosomal subunits
Mitochondrial small ribosomal subunits
Mitochondrial tRNA synthase
Mitochondrial translation initiation/elongation factors
Other mitochondrial translation factors
Mitochondrial transcription
Mitochondrial import
Mitochondrial transporter
TCA cycle
Lipid metabolism
Iron sulfur cluster biogenesis
Complex I ETC
Complex II ETC
Complex III ETC
Complex IV ETC
Complex V ETC
Cytochrome c
Mitochondrial proteases
Mitochondrial chaperonnes
ETC assembly factors
Mitochondrial dynamics and ultrastructure
Mitochondrial proteins with no obvious homolog in human

0   10   20   30
Number of genes

E

Phsp-6GFP Fluorescence Intensity (A.U.)

tag-208, mrpl-9, mrps-12, dars-2, gfm-1, mma-1, tomm-20, mtch-1, dlst-1, acdh-13, Y39B6A.3, F53F4.10*, sdhd-1*, cyc-1*, W09C5.8, atp-5, cyc-2.1, spg-7, hsp-60, sco-1, eat-3, Y54G11A.17

F

Phsp-60GFP Fluorescence Intensity (A.U.)

tag-208, mrpl-9, mrps-12, dars-2, gfm-1, mma-1, tomm-20, mtch-1, dlst-1, acdh-13, Y39B6A.3, F53F4.10, sdhd-1, cyc-1, W09C5.8, atp-5, cyc-2.1, spg-7, hsp-60, sco-1, eat-3, Y54G11A.17

G

Relative *Phsp-6GFP* fluorescence intensity(A.U.)

■ tag-208(RNAi)   ■ atfs-1(RNAi)

mrpl-9, mrps-12, dars-2, gfm-1, mma-1, tomm-20, mtch-1, dlst-1, acdh-13, Y39B6A.3, F53F4.10, sdhd-1, cyc-1, W09C5.8, atp-5, cyc-2.1, spg-7, hsp-60, sco-1, eat-3, Y54G11A.17

H

Relative *Phsp-6GFP* fluorescence intensity(A.U.)

■ +/+   ■ gcn-2(ok871)

mrpl-9, mrps-12, dars-2, gfm-1, mma-1, tomm-20, mtch-1, dlst-1, acdh-13, Y39B6A.3, F53F4.10, sdhd-1, cyc-1, W09C5.8, atp-5, cyc-2.1, spg-7, hsp-60, sco-1, eat-3, Y54G11A.17

Figure 1. Genome-wide RNAi Screen Identifies Genes Required for the Maintenance of Mitochondrial Homeostasis

(A) Percentage of genes identified in our screen previously implicated or not in UPRmt.
(B) Percentage of genes in the entire genome (Shaye and Greenwald, 2011) or among the genes identified in our screen with human orthologs.
(C) Overlap between genes of the GO "mitochondrion" and genes identified in our screen.
(D) The 171 candidates identified were grouped into 22 mitochondrial processes.

(legend continued on next page)

but not all, mitochondrial processes triggers UPR[mt] that is dependent on ATFS-1 but not antagonized by GCN-2. Interestingly, some of these mitochondrial processes are not predicted to directly cause a mito-nuclear imbalance when blocked. Instead, they are predicted to cause a decrease in mitochondrial membrane potential. Therefore, we propose that a decrease in mitochondrial membrane potential acts as a signal that triggers UPR[mt]. Furthermore, we propose that the mitochondrial targeting sequence (MTS) of ATFS-1 acts as a sensor for changes in mitochondrial membrane potential. Consistent with this model, we demonstrate that the "weak" MTS of ATFS-1 is essential for its ability to sense a decrease in mitochondrial membrane potential and to activate UPR[mt].

RESULTS

Genome-wide RNAi Screen for Genes that Induce UPR[mt] When Knocked Down

To systematically identify *C. elegans* genes that induce UPR[mt] when knocked down, we performed a genome-wide RNAi screen covering ≥90% of annotated *C. elegans* genes (Kamath and Ahringer, 2003). UPR[mt] induction was monitored with a *hsp-6* HSP70 transcriptional reporter (P*hsp-6*GFP) (Yoneda et al., 2004). We identified 198 "inducer" genes that reproducibly cause the upregulation of the P*hsp-6*GFP reporter when knocked down. Among these, 171 encode proteins that have been shown to localize to mitochondria or are predicted to do so (Table S1A). We refer to this subset as the "mitochondrial inducers" and have focused our analyses on this group of genes.

The mitochondrial inducers encode proteins that represent each of the four major mitochondrial sub-compartments. Most of these genes have human orthologs (95%) and have not previously been identified as affecting UPR[mt] (56%) (Bennett et al., 2014; Runkel et al., 2013) (Figures 1A and 1B). The inducers include 96 of the 424 genes in the Gene Ontology (GO) category "mitochondrion" (Figure 1C). Although the remaining 75 genes do not belong to this GO category, they encode proteins that have been shown, or are predicted, to localize to mitochondria. Concerning the remaining 328 genes that belong to the GO category "mitochondrion" and that we did not identify, we cannot exclude that we missed some because of RNAi efficiency. However, as shown below, compromising certain mitochondrial processes does not induce UPR[mt]. In order to assess the specific nature and diversity of processes affected by the mitochondrial inducers, we analyzed all 57 sub-GO groups included in the GO category "mitochondrion." We found that the genes we identified are associated with 44 of these sub-GO groups and that 5 of these sub-GO groups were not previously identified as inducing UPR[mt] when compromised (Table S1B).

Compromising Mitochondrial Ca²⁺ Homeostasis or Mitophagy Fails to Induce UPR[mt]

The 13 sub-GO groups not represented by any of the 171 genes we identified include a total of 19 genes. We retested the 14 genes present in the RNAi library (Kamath and Ahringer, 2003) and identified two additional genes that induce P*hsp-6*GFP expression when knocked down (Table S1C).

Mitochondrial Ca²⁺ homeostasis is one of the mitochondrial processes that did not induce UPR[mt] when compromised. The sub-GO group "mitochondrial Ca²⁺ homeostasis" contains two genes: *mcu-1* and *emre-1*. In order to confirm our RNAi results, we analyzed animals carrying the *mcu-1* mutation *ju1154* (Xu and Chisholm, 2014) and showed that the loss of *mcu-1* does not induce the expression of the P*hsp-6*GFP reporter, confirming that compromising mitochondrial Ca²⁺ homeostasis does not trigger UPR[mt] (Figure S1A). Mitophagy (Pickrell and Youle, 2015) is another process that was not identified in our screen. Accumulation of misfolded proteins in the mitochondrial matrix of cultured mammalian cells has been shown to trigger PINK1- and Parkin-dependent mitophagy (Jin and Youle, 2013). We analyzed animals carrying a deletion in the *C. elegans* Parkin gene *pdr-1*, *lg103* (Springer et al., 2005) and animals carrying a deletion in the *C. elegans* PINK1 gene *pink-1*, *tm1779* (Sämann et al., 2009) and found that neither mutation induces the P*hsp-6*GFP reporter (Figures S1B–S1E). In addition, the upregulation of the P*hsp-6*GFP reporter by *spg-7(RNAi)* is not significantly affected by *pink-1(tm1779)* or *pdr-1(lg103)* (*spg-7* encodes the *C. elegans* homolog of the mitochondrial quality control protease AFG3L2). Finally, we did not observe any induction of the P*hsp-6*GFP reporter upon the knockdown of the gene *dct-1*, which encodes the *C. elegans* BNIP3 homolog, thought to be required for mitophagy (Palikaras et al., 2015) (Table S1C). Thus, not all mitochondrial processes trigger UPR[mt] activation when compromised.

UPR[mt] Induced by Compromising Most Mitochondrial Processes Is Dependent on ATFS-1 but Is Not Antagonized by the Kinase GCN-2

We divided the 171 mitochondrial inducers into 22 groups on the basis of their roles in specific mitochondrial processes (Figure 1D). For most of the 22 groups, we selected one representative gene and quantified the induction of the P*hsp-6*GFP reporter (Figure 1E). As a negative control, we knocked down *tag-208*, which encodes the *C. elegans* homolog of human Sorbin and does not induce UPR[mt] when knocked down (Figures S1F and S1G). To confirm that the observed effects are not specific to *hsp-6* HSP70, we also quantified induction of a *hsp-60* HSP60 transcriptional reporter (P*hsp-60*GFP) (Yoneda et al., 2004). With the exception of *sdhd-1*, knockdown of all genes caused P*hsp-60*GFP upregulation (Figure 1F).

(E and F) Effect of the knockdown of one candidate for each mitochondrial process on the (E) P*hsp-6*GFP and (F) P*hsp-60*GFP reporters. Reporter expression was monitored by fluorescence microscopy and quantified (n = 2-3;mean and SD are shown; *RNAi was diluted with *tag-208(RNAi)*).
(G) Double RNAi with *tag-208(RNAi)* or *atfs-1(RNAi)*. Reporter expression was monitored by fluorescence microscopy and quantified (n = 2-3; mean and SD are shown).
(H) Knockdown was performed in wild-type (+/+) or a strain carrying *gcn-2(ok871)*. Reporter expression was monitored by fluorescence microscopy and quantified (n = 2–6; mean and SD are shown; *RNAi was diluted with *tag-208(RNAi)*).
In all panels, n is the number of biological replicates.
See also Table S1 and Figures S1 and S2.

Next, we tested whether UPR^mt induced by compromising the mitochondrial processes identified is dependent on the transcription factor ATFS-1 (Nargund et al., 2012). To that end, we performed double RNAi experiments with the representative genes and either *atfs-1(RNAi)* or, as a control, *tag-208(RNAi)*. Double RNAi of any of the genes with *tag-208(RNAi)* induced the upregulation of the P*hsp-6*GFP reporter (Figure 1G, gray bars). In contrast, double RNAi of any of the genes with *atfs-1(RNAi)* resulted in the complete suppression of the upregulation (black bars). We also tested whether the kinase GCN-2 plays a role in the induction of UPR^mt upon inactivation of the genes identified in our screen. To that end, we used a strain carrying the *gcn-2* loss-of-function mutation *ok871*. As shown in Figure 1H, for the genes tested, the upregulation of the P*hsp-6*GFP reporter observed in wild-type animals (gray bars) was similar to that observed in *gcn-2(ok871)* mutant animals (black bars). We confirmed this result with an independent loss-of-function mutation *gcn-2(ok886)* (Figures S2A and S2B). In contrast, activation of the P*hsp-6*GFP reporter by the loss-of-function mutation *clk-1(qm30)* (*clk-1* is required for ubiquinone synthesis) is enhanced by knockdown of *gcn-2* (Figure S2C), as published previously (Baker et al., 2012). Therefore, UPR^mt induced by compromising most mitochondrial processes is dependent on ATFS-1 but is not antagonized by the kinase GCN-2.

UPR^mt Is Triggered by Compromising Mitochondrial Processes that Are Required for the Maintenance of the Mito-nuclear Balance

The GO category "mitochondrial translation" is significantly enriched in our dataset (Table S1D). Among genes present in the RNAi library (Kamath and Ahringer, 2003), we identified 75% of the large subunits of the mitochondrial ribosome (*mrpl* genes) and ∼96% of the small subunits of the mitochondrial ribosome (*mrps* genes). Furthermore, we also found nine genes encoding mitochondrial aminoacyl tRNA synthetases, and genes encoding mitochondrial translation initiation and elongation factors.

The GO category "protein import into mitochondrial matrix" is also significantly enriched in our dataset (Table S1D). We identified components of the TOM and TIM complexes (Figures 2A and 2B). (Some were previously identified as inducers of UPR^mt; Bennett et al., 2014; Runkel et al., 2014). We also confirmed that the knockdown of *timm-23*, which encodes the major subunit of the TIM23 complex, induces UPR^mt. We also identified *gop-3* and *tin-9.1*, which encode the homolog of the human SAMM50 protein, and the homolog of the small Tim protein Tim9, respectively (Figures 2A and 2B). Tim9 functions as a chaperone in the intermembrane space and assists beta-barrel proteins in reaching the SAM complex to be inserted into the outer mitochondrial membrane (OMM) (Wiedemann and Pfanner, 2017; Wiedemann et al., 2004). Tim9 also assists carrier proteins in reaching the TIM22 complex to be inserted into the IMM (Adam et al., 1999; Wiedemann and Pfanner, 2017). These two aspects of mitochondrial protein import were not previously identified as inducing UPR^mt when compromised.

Finally, we found that the knockdown of the nuclear-encoded subunits of complex I, III, IV, or V of the ETC also triggers UPR^mt and that several GO categories associated with ETC complexes are significantly enriched in our dataset. (Table S1D). Further-

more, we found that compromising assembly of complex I, III, or IV also leads to UPR^mt activation (e.g., by knockdown of *nuaf-1*, which encodes the homolog of the human complex I assembly factor NDUFAF1; *bcs-1*, which encodes the homolog of the human complex III assembly factor BCS1L; or *cox-14*, which encodes the homolog of the human complex IV assembly factor COX14; see Table S1).

The identification of mitochondrial translation, import and ETC as mitochondrial processes that when compromised induce UPR^mt is consistent with mito-nuclear imbalance and the resulting accumulation of unassembled subunits of ETC complexes being the signal that triggers UPR^mt (Houtkooper et al., 2013).

Mitochondrial Processes that Are Not Required for the Maintenance of the Mito-nuclear Balance Also Trigger UPR^mt When Compromised

We found that the knockdown of the cytochrome *c* gene *cyc-2.1* induces UPR^mt. The knockdown of *cyc-2.1* presumably causes a defect in the activity of the ETC; however, it is not predicted to directly cause mito-nuclear imbalance. In addition, we identified genes encoding subunits of complex II (*sdha-1*, *sdhd-1*, and *sdhc-1*). Although knockdown of these genes may cause an accumulation of other complex II subunits, it does not cause mito-nuclear imbalance, because all subunits of complex II are encoded in the nuclear genome. To test whether knockdown of any subunit of complex II induces UPR^mt, we individually knocked down the genes encoding all four subunits. As shown in Figures 2C and 2D, knockdown of any of these genes induces upregulation of the P*hsp-6*GFP reporter. We also found that the level of endogenous HSP-6 protein but not HSP-60 protein significantly increases upon *sdhc-1(RNAi)* (Figure S3). Hence, compromising the ETC is sufficient to trigger UPR^mt.

The GO category "tricarboxylic acid cycle" is significantly enriched in our dataset (Table S1D). We identified several genes encoding subunits of enzymes of the tricarboxylic acid (TCA) cycle (Table S1A). Reduced levels of these proteins may lead to the disruption of the stoichiometry of their respective TCA complexes, thereby leading to the accumulation of unassembled proteins in the mitochondrial matrix. Alternatively, UPR^mt might also be triggered by the dysfunction of the TCA cycle itself. To test this hypothesis, we knocked down genes encoding the remaining enzymes of the TCA cycle. Knockdown of *aco-2*, *idha-1*, *cts-1*, *mdh-2*, and *fum-1* induce the P*hsp-6*GFP reporter (Figure 3). We also found that the level of endogenous HSP-6 protein but not HSP-60 protein tends to slightly increase albeit not significantly upon *fum-1(RNAi)* (Figure S3) (It should be noted that because HSP-6 and HSP-60 are highly abundant proteins (Bensaddek et al., 2016), even small changes represent substantial changes in protein amounts. Furthermore, the basal expression level of P*hsp-6*GFP is low in contrast to the high basal level of endogenous HSP-6 protein. Hence, the fold change of P*hsp-6*GFP is likely an overestimation of the fold change of HSP-6. Finally, although tubulin is ubiquitously expressed, the UPR^mt transcriptional reporters are expressed mostly in intestinal cells. Hence, it is possible that UPR^mt is restricted to certain tissues. The HSP-6/tubulin or HSP-60/tubulin ratio might therefore underestimate the upregulation of HSP-6 or HSP-60 in the cells in which UPR^mt occurs. Such
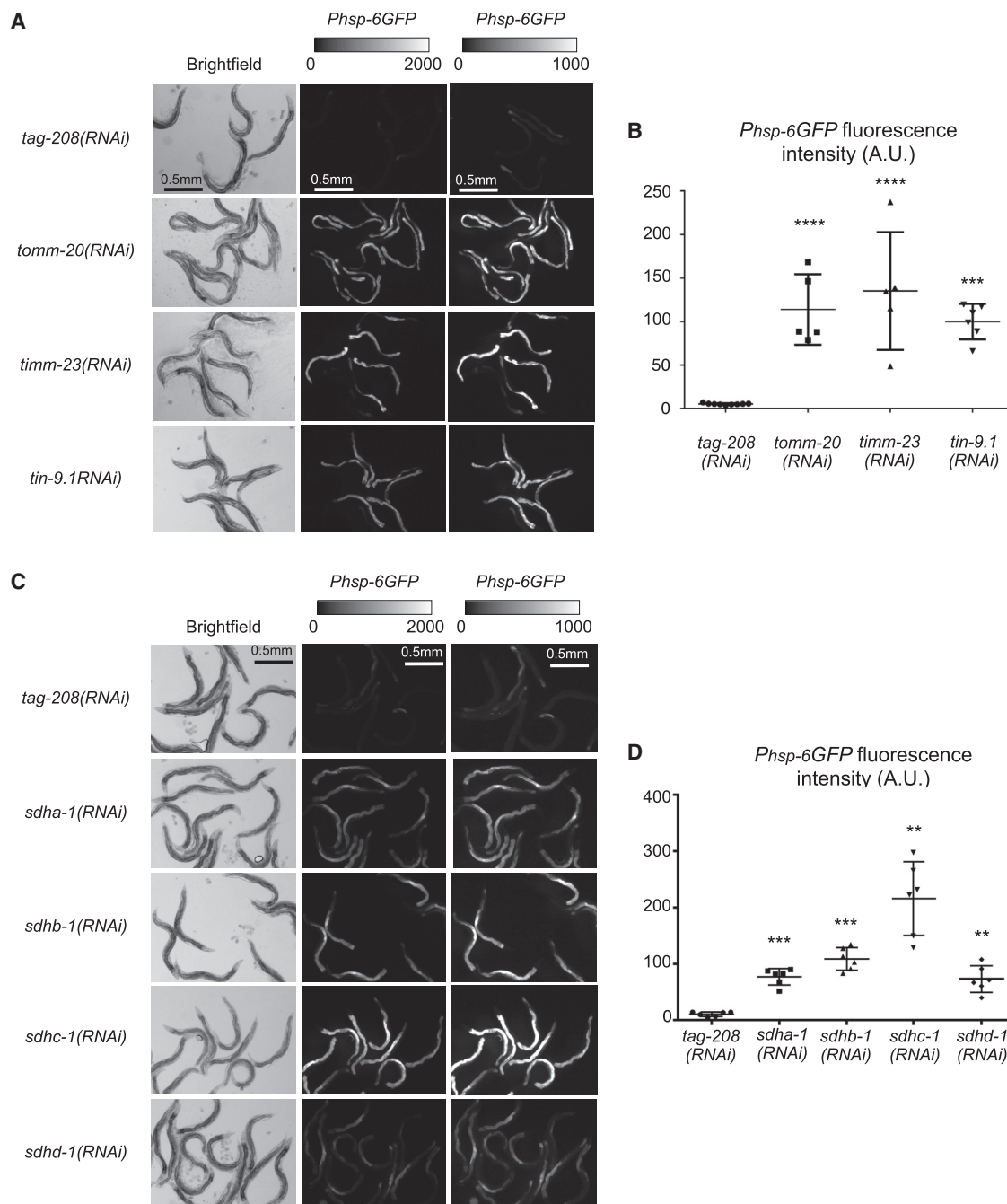
Figure 2. Knockdown of Mitochondrial Import Machinery or Complex II Induces UPR^mt

(A and C) Bright-field and fluorescence images of the P$_{hsp-6}$GFP reporter strain after different RNAi treatment to knock down the mitochondrial import machinery (A) or complex II subunits (C). Two intensity scales are shown.

(B and D) Quantification of P$_{hsp-6}$GFP fluorescence intensity (n ≥ 5; n is the number of biological replicates; mean and SD are shown; for B, ***p < 0.001 and ****p < 0.0001 by one-way ANOVA with Bonferroni's multiple-comparison test to tag-208(RNAi); for D, **p < 0.01 and ***p < 0.001 by Welch's ANOVA with Games-Howell post hoc test to tag-208(RNAi)).

See also Figure S3.

an underestimation might affect HSP-60 more strongly than HSP-6, as hsp-60 is less strongly transcriptionally upregulated upon mitochondrial stress than hsp-6 (Haynes et al., 2007). Because CTS-1, FUM-1, and MDH-2 are homo-oligomeric en-zymes, reduction in their levels will not cause proteotoxic stress. It will, however, cause a decrease in the activity of the TCA cycle. Hence, compromising the TCA cycle is sufficient to trigger UPR^mt.
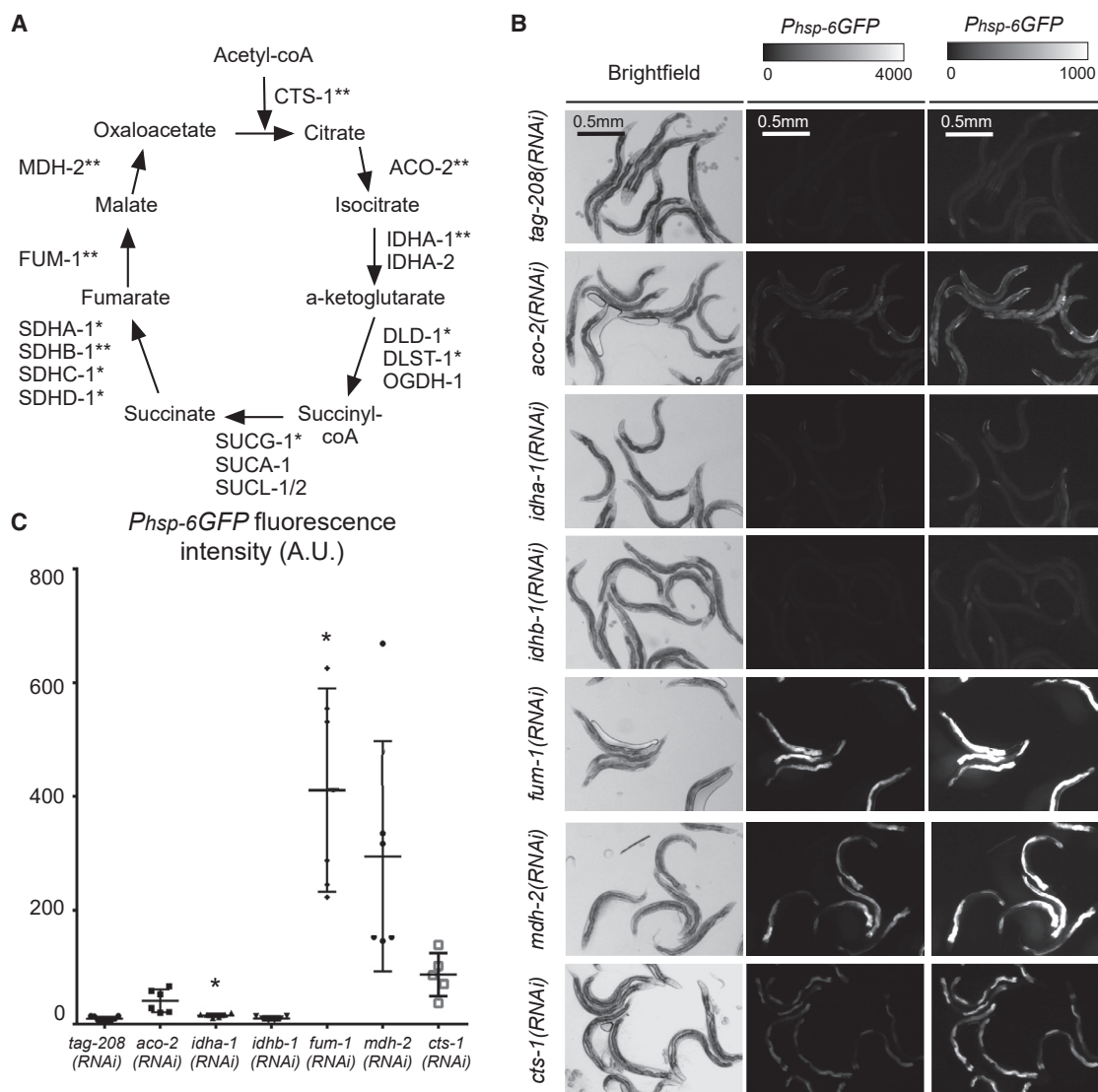
Figure 3. Knockdown of Any Enzyme of TCA Cycle Induces UPR^mt

(A) TCA cycle. Single and double asterisks indicate genes identified in our screen and subsequent experiments, respectively.

(B) Bright-field and fluorescence images of P$_{hsp-6}$GFP reporter strain after different RNAi treatment. Two intensity scales are shown.

(C) Quantification of P$_{hsp-6}$GFP fluorescence intensity (n ≥ 5; n is the number of biological replicates; mean and SD are shown; *p < 0.05 by Welch's ANOVA with Games-Howell post hoc test to *tag-208(RNAi)*).

See also Figures S3 and S4.

We also identified genes encoding proteins required for lipid catabolism (e.g., *ard-1*, *ech-6*, and *acdh-13* encode three mitochondrial beta-oxidation enzymes). The GO category "fatty acid biosynthetic process" is also enriched in our dataset (Table S1D). We identified two genes (*pgs-1* and *mdmh-35)* that encode proteins involved in cardiolipin (CL) biosynthesis, a lipid biosynthetic pathway that was not identified before as inducing UPR^mt when compromised. To confirm this result, we tested *crls-1*, which encodes CL synthase, and found that its knockdown induces the P$_{hsp-6}$GFP reporter expression (Figure S4). To test whether the biosynthesis of other lipids also induces UPR^mt, we tested *psd-1*, which encodes phosphatidylserine decarbox-

ylase and plays a role in the biosynthesis of phosphatidylethanol-amine (PE) (Osman et al., 2011). We found that knockdown of *psd-1* also induces P$_{hsp-6}$GFP reporter expression (Figure S4). Hence, compromising lipid metabolism triggers UPR^mt.

A Reduction in Mitochondrial Membrane Potential Correlates with the Induction of UPR^mt

Rather than directly causing mito-nuclear imbalance, the processes described above are predicted to cause a reduction in mitochondrial membrane potential. Although compromising the ETC directly causes a decrease in mitochondrial membrane potential, compromising the TCA cycle leads to a decrease in the
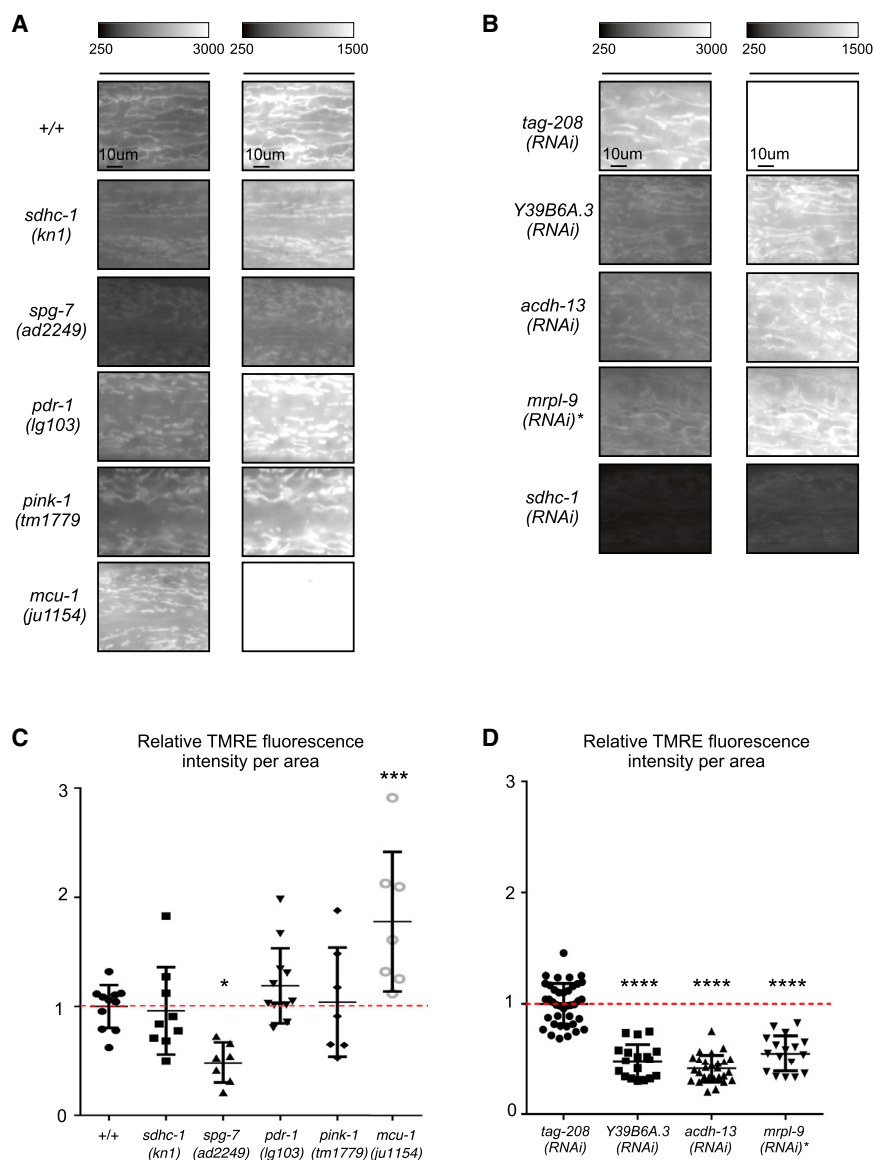
Figure 4. Genes that Induce UPRmt When Knocked Down Are Required to Maintain Mitochondrial Membrane Potential

(A) Wild-type (+/+) or animals carrying different loss-of-function mutations were stained with TMRE. Representative images of mitochondria in hypodermal cells are shown with two intensity scales.

(B) Wild-type subjected to different RNAi (mrpl-9(RNAi) was diluted with tag-208(RNAi)) were stained with TMRE. Representative images of mitochondria in hypodermal cells are shown with two intensity scales.

(C and D) Quantification of TMRE fluorescence intensity per area (C, n ≥ 7; D, n ≥ 17; n is the number of animals analyzed; mean and SD are shown; *p < 0.05, ***p < 0.001, and ****p < 0.0001 by one-way ANOVA with Bonferroni's multiple-comparison test to tag-208(RNAi) or +/+; sdhc-1(RNAi) with data was not quantified, as the signal was too low to be detected by the segmentation macro; for mcu-1(ju1154) and tag-208(RNAi) the 250–1,500 intensity images are white because of saturation.

NADH level, resulting in a decrease in ETC function and, consequently, a reduction in mitochondrial membrane potential. Furthermore, compromising beta-oxidation causes a reduction in the level of acetyl-CoA entering the TCA cycle, indirectly causing a reduction in mitochondrial membrane potential. Finally, compromising CL biosynthesis has been shown to affect the formation of respiratory supercomplex in *S. cerevisiae* (Pfeiffer et al., 2003). Although this indirectly leads to proteotoxic stress, it also causes a reduction in mitochondrial membrane potential (Jiang et al., 2000). Finally, compromising PE biosynthesis in *S. cerevisiae* has been shown to cause a decrease in mitochondrial membrane potential (Böttinger et al., 2012).

To test whether genes that induce UPRmt when knocked down are required to maintain mitochondrial membrane potential, using the mitochondrial potential-sensitive dye TMRE, we stained animals in which some of these genes had been knocked down by mutation or RNAi and measured TMRE fluorescence intensity per area in mitochondria in hypodermal cells. We found that the knockdown of any of the genes tested results in a lower average mitochondrial TMRE fluorescence intensity. (Figure 4). The mitochondrial TMRE fluorescence intensity is proportional to mitochondrial membrane potential (Loew et al., 1993), indicating that the loss of genes that induce UPRmt when knocked down results in a reduction in mitochondrial membrane potential. In contrast, animals carrying loss-of-function mutations in genes that do not induce UPRmt when knocked down (such as pdr-1(lg103), pink-1(tm1779), or mcu-1(ju1154)), do not exhibit a lower average mitochondrial TMRE fluorescence intensity and therefore do not exhibit a reduction of mitochondrial membrane potential (Figure 4). Therefore, there is a correlation between a reduction in mitochondrial membrane potential and the induction of UPRmt.

The MTS of ATFS-1 Acts as a Sensor for Mitochondrial Membrane Potential

Mitochondrial protein import is sensitive to mitochondrial membrane potential and depends on the net charge of the MTS (Martin et al., 1991). Mitochondrial proteins containing a MTS with a low net charge can only be imported into mitochondria with a high membrane potential. However, mitochondrial proteins containing a MTS with a high net charge can be imported even into mitochondria with a low membrane potential. The MTS of ATFS-1 has a lower net charge (+4) than that of
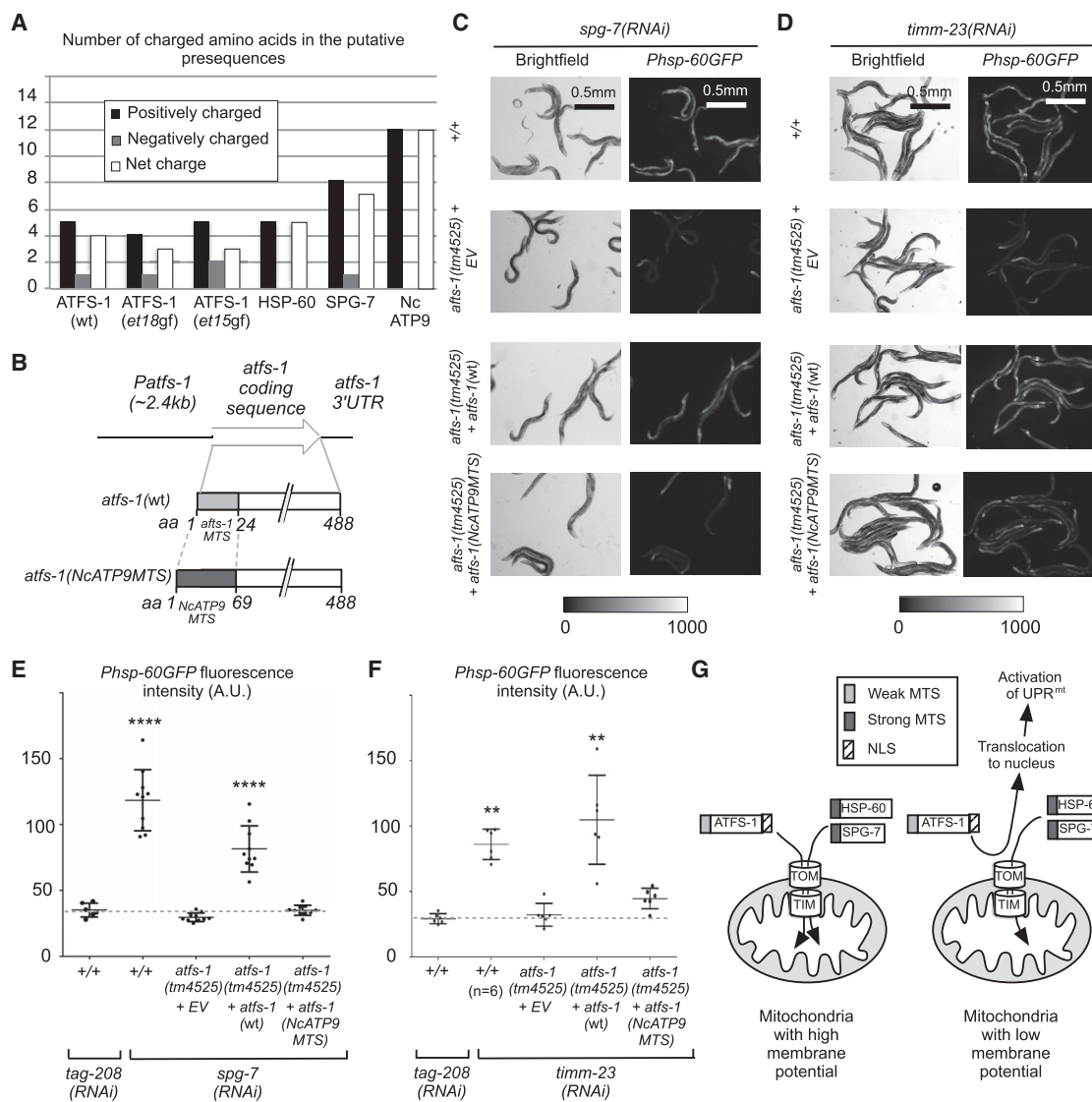
Figure 5. The Weak MTS of ATFS-1 Is Necessary for the Ability of ATFS-1 to Act as a Sensor of UPR^mt

(A) Analysis of the MTS of *C. elegans* ATFS-1(WT), ATFS-1(*et15*), ATFS-1(*et18*), HSP-60(WT), SPG-7(WT), and *N. crassa* ATP9.

(B) Schematic of the constructs. The MTS of ATFS-1 was replaced with the MTS of ATP synthase subunit 9 of *N. crassa* in the *atfs-1*(*NcATP9MTS*) construct.

(C) All strains carry the P$_{hsp-60}$GFP reporter. Wild-type (+/+) and *atfs-1*(*tm4525*) animals carrying the empty vector (EV), the *atfs-1*(WT) transgene, or the *atfs-1*(*NcATP9MTS*) transgene were treated with *spg-7*(*RNAi*) and analyzed by bright-field and fluorescence microscopy.

(D) Strains indicated in (C) were treated with *timm-23*(*RNAi*).

(E and F) Quantification of P$_{hsp-60}$GFP fluorescence intensity (n ≥ 6; n = number of biological replicates; mean and SD are shown; for E, ****p < 0.0001 by Welch's ANOVA with Games-Howell post hoc test to +/+ with *tag-208*(*RNAi*); for F, **p < 0.01 by Kruskal-Wallis with Dunn's multiple-comparisons test to +/+; *tag-208*(*RNAi*)).

(G) Model of activation of UPR^mt.

See also Figure S5.

HSP-60 (+5) or SPG-7 (+7) (Figure 5A). Animals carrying the *atfs-1* mutations *et15*gf or *et18*gf exhibit constitutive activation of UPR^mt. Interestingly, both mutations result in a reduction in the net charge of the MTS and presumably a reduction in mitochondrial import (Rauthan et al., 2013). Thus, we hypothesized that a decrease in mitochondrial membrane potential reduces the efficiency with which ATFS-1, but not HSP-60 or SPG-7, is imported into mitochondria.

To test this hypothesis we generated transgenic lines that express either a wild-type *atfs-1* rescuing construct (Figure 5B, *atfs-1*(WT) [wild-type]) or a rescuing construct encoding a modified ATFS-1 protein (ATFS-1(NcATP9MTS)), in which the N-terminal 24 amino acids have been replaced with the N-terminal 69 amino acids of the ATP synthase subunit 9 of *Neurospora crassa*, which is a strong MTS with a net charge of +12 (Figures 5A and 5B).

We found that the *atfs-1*(WT) transgene partially rescues the *atfs-1(tm4525)* phenotype, restoring induction of the P$_{hsp-60}$GFP reporter upon *spg-7(RNAi)* (Figures 5C and 5E). In contrast, we found that the *atfs-1(NcATP9MTS)* transgene fails to restore the induction of the P$_{hsp-60}$GFP reporter upon *spg-7(RNAi)*, although the levels of ATFS-1(NcATP9MTS) and ATFS-1(WT) proteins were similar (Figure S5). Hence, the ATFS-1(NcATP9MTS) protein is unable to activate UPR^{mt} in response to mitochondrial stress caused by *spg-7(RNAi)*. We speculate that ATFS-1(NcATP9MTS) import is very efficient and not affected by a partial reduction in mitochondrial membrane potential caused by the loss of *spg-7* function. As a further test, we knocked down the gene *timm-23*, which compromises mitochondrial protein import directly. The strain carrying the *atfs-1*(WT) transgene fully restored the induction of the P$_{hsp-60}$GFP reporter upon *timm-23(RNAi)*. Furthermore, we observed a partial rescue of P$_{hsp-60}$GFP induction even in the strain carrying the *atfs-1(NcATP9MTS)* transgene (Figures 5D and 5F). Hence, in response to higher levels of mitochondrial stress (i.e., when mitochondrial import is directly compromised) ATFS-1(NcATP9MTS) is able to activate UPR^{mt}. Although this result supports our model, it also demonstrates that the ATFS-1(NcATP9MTS) protein is able to activate the transcriptional reporter and therefore is a functional transcription factor. On the basis of these findings, we propose that a reduction in mitochondrial membrane potential acts as a signal for the induction of UPR^{mt} and that the MTS of ATFS-1 acts as a sensor for this signal.

DISCUSSION

Similar to other UPRs, UPR^{mt} was proposed to be triggered by the accumulation of unfolded proteins (Yoneda et al., 2004). Although several lines of evidence are consistent with unfolded protein stress being the signal that triggers UPR^{mt} (Haynes et al., 2007, 2010; Houtkooper et al., 2013), it has so far only been shown in mammalian cells that a misfolded mitochondrial matrix protein can trigger it (Zhao et al., 2002). It has recently been noted that all perturbations known to induce UPR^{mt} are also likely to reduce mitochondrial import efficiency (Melber and Haynes, 2018). Therefore, it has been proposed that under these conditions, ATFS-1 relocalizes to the nucleus and activates UPR^{mt}. In order to better understand which signal triggers UPR^{mt}, we performed a genome-wide RNAi screen to systematically identify mitochondrial processes that induce UPR^{mt} when compromised.

Our results demonstrate that most mitochondrial processes trigger UPR^{mt} when compromised. Therefore, most mitochondrial processes are required for the maintenance of mitochondrial homeostasis. However, some processes, such as mitophagy, do not appear to be required. In addition, we found that a block in mitophagy has no effect on the induction of UPR^{mt}. Haynes and co-workers have proposed that UPR^{mt} is the first line of defense that can help mitochondria to regain homeostasis. If this line of defense fails, mitophagy is activated to eliminate irremediably damaged mitochondria (Pellegrino et al., 2013). Our data show that the converse is not the case (i.e., a block in mitophagy does not induce UPR^{mt}).

Our unbiased genome-wide approach confirms that blocking mitochondrial import leads to the activation of UPR^{mt}. Although the knockdown of components of the TOM or TIM23 complexes directly affects the import of ATFS-1, the effect of the knockdown of the small Tim protein Tim9 on ATFS-1 is likely indirect, because Tim9 is not involved in the import of mitochondrial matrix targeted protein. We also show that UPR^{mt} is induced in response to compromising mitochondrial processes (electron transport, TCA cycle, lipid catabolism, CL and PE biosynthesis) that are predicted to be required for the maintenance of mitochondrial membrane potential, but not for the maintenance of mito-nuclear balance. Furthermore, compromising any of the other mitochondrial processes that we identified in our screen is expected to at least indirectly reduce mitochondrial membrane potential. Although we cannot exclude that a decrease in mitochondrial ATP levels caused by a reduction in mitochondrial membrane potential participates in the activation of UPR^{mt} (because ATP is required for protein folding as well as mitochondrial import), we propose that a reduction in mitochondrial membrane potential is a general signal for the induction of UPR^{mt}. Consistent with this model, drugs known to cause a reduction in mitochondrial membrane potential (such as rotenone or antimycin) (Johnson et al., 1981) have been shown to induce UPR^{mt} (Liu et al., 2014; Runkel et al., 2013). Finally, it was shown that the induction of UPR^{mt} upon *spg-7(RNAi)* is partially dependent on the transporter HAF-1 (Haynes et al., 2010). Our model is still compatible with a role of HAF-1 in the UPR^{mt} pathway. We speculate that because peptides exported by HAF-1 are most likely charged, they may affect mitochondrial membrane potential when exported. Such peptides may also affect mitochondrial protein import as recently shown with isolated mammalian mitochondria *in vitro* (Oliveira and Hood, 2018).

Bioinformatic analysis revealed that the MTS of ATFS-1 is weaker than that of other mitochondrial proteins, such as HSP-60 or SPG-7. Furthermore, in contrast to HSP-60 and SPG-7, ATFS-1 additionally contains a C-terminal nuclear localization sequence (NLS). We propose that the combination of the NLS and the relative "weakness" of the MTS is essential for ATFS-1's function as a UPR^{mt} sensor. To test this, we generated a chimeric ATFS-1 protein containing a strong MTS and showed that this protein is unable to induce UPR^{mt} in response to lower levels of mitochondrial stress (i.e., *spg-7(RNAi)*) but is able to induce UPR^{mt} in response to higher levels of mitochondrial stress (i.e., *timm-23(RNAi)*). We speculate that this chimeric ATFS-1 protein is unable to act as a UPR^{mt} sensor in response to lower levels of mitochondrial stress because its import is very efficient and not affected by a decrease in mitochondrial membrane potential caused by *spg-7(RNAi)*. We propose a model in which defects in most mitochondrial processes lead to a decrease in mitochondrial membrane potential, which blocks the import of ATFS-1, thereby causing its relocalization to the nucleus. The effectors of UPR^{mt}, such as HSP-60 and SPG-7, can still be imported into these compromised mitochondria because their MTSs are stronger than that of ATFS-1 (Figure 5G). Consistent with this model, we demonstrated that UPR^{mt} induced by a defect in any of the mitochondrial processes identified in our screen is dependent on ATFS-1. In conclusion, we propose that

the predominant signal triggering UPR^{mt} is a decrease in mito-chondrial membrane potential, which is sensed by the MTS of ATFS-1.

STAR★METHODS

Detailed methods are provided in the online version of this paper and include the following:

- KEY RESOURCES TABLE
- LEAD CONTACT AND MATERIALS AVAILABILITY
- EXPERIMENTAL MODEL AND SUBJECT DETAILS
  - *C. elegans* strains and culture conditions
  - Transgenic lines generation
- METHOD DETAILS
  - Genome wide RNA interference screen
  - Bioinformatic analysis
  - Further analysis of the candidates
  - Analysis of HSP-6 and HSP-60 protein levels
  - TMRE staining and quantification
- QUANTIFICATION AND STATISTICAL ANALYSIS
- DATA AND CODE AVAILABILITY

REFERENCES

Adam, A., Endres, M., Sirrenberg, C., Lottspeich, F., Neupert, W., and Brunner, M. (1999). Tim9, a new component of the TIM22.54 translocase in mitochondria. EMBO J. *18*, 313–319.

Baker, B.M., Nargund, A.M., Sun, T., and Haynes, C.M. (2012). Protective coupling of mitochondrial function and protein synthesis via the eIF2α kinase GCN-2. PLoS Genet. *8*, e1002760.

Bennett, C.F., Vander Wende, H., Simko, M., Klum, S., Barfield, S., Choi, H., Pineda, V.V., and Kaeberlein, M. (2014). Activation of the mitochondrial unfolded protein response does not predict longevity in *Caenorhabditis elegans*. Nat. Commun. *5*, 3483.

Bensaddek, D., Narayan, V., Nicolas, A., Murillo, A.B., Gartner, A., Kenyon, C.J., and Lamond, A.I. (2016). Micro-proteomics with iterative data analysis: proteome analysis in *C. elegans* at the single worm level. Proteomics *16*, 381–392.

Böttinger, L., Horvath, S.E., Kleinschroth, T., Hunte, C., Daum, G., Pfanner, N., and Becker, T. (2012). Phosphatidylethanolamine and cardiolipin differentially affect the stability of mitochondrial respiratory chain supercomplexes. J. Mol. Biol. *423*, 677–686.

Brenner, S. (1974). The genetics of *Caenorhabditis elegans*. Genetics *77*, 71–94.

Claros, M.G., and Vincens, P. (1996). Computational method to predict mito-chondrially imported proteins and their targeting sequences. Eur. J. Biochem. *241*, 779–786.

Durieux, J., Wolff, S., and Dillin, A. (2011). The cell-non-autonomous nature of electron transport chain-mediated longevity. Cell *144*, 79–91.

Fiorese, C.J., Schulz, A.M., Lin, Y.F., Rosin, N., Pellegrino, M.W., and Haynes, C.M. (2016). The transcription factor ATF5 mediates a mammalian mitochondrial UPR. Curr. Biol. *26*, 2037–2043.

Gardner, B.M., Pincus, D., Gotthardt, K., Gallagher, C.M., and Walter, P. (2013). Endoplasmic reticulum stress sensing in the unfolded protein response. Cold Spring Harb. Perspect. Biol. *5*, a013169.

Hadwiger, G., Dour, S., Arur, S., Fox, P., and Nonet, M.L. (2010). A monoclonal antibody toolkit for *C. elegans*. PLoS ONE *5*, e10161.

Haynes, C.M., Petrova, K., Benedetti, C., Yang, Y., and Ron, D. (2007). ClpP mediates activation of a mitochondrial unfolded protein response in *C. elegans*. Dev. Cell *13*, 467–480.

Haynes, C.M., Yang, Y., Blais, S.P., Neubert, T.A., and Ron, D. (2010). The matrix peptide exporter HAF-1 signals a mitochondrial UPR by activating the transcription factor ZC376.7 in *C. elegans*. Mol. Cell *37*, 529–540.

Honda, S., Ishii, N., Suzuki, K., and Matsuo, M. (1993). Oxygen-dependent perturbation of life span and aging rate in the nematode. J. Gerontol. *48*, B57–B61.

Houtkooper, R.H., Mouchiroud, L., Ryu, D., Moullan, N., Katsyuba, E., Knott, G., Williams, R.W., and Auwerx, J. (2013). Mitonuclear protein imbalance as a conserved longevity mechanism. Nature *497*, 451–457.

Huang, W., Sherman, B.T., and Lempicki, R.A. (2009). Systematic and integrative analysis of large gene lists using DAVID bioinformatics resources. Nat. Protoc. *4*, 44–57.

Jiang, F., Ryan, M.T., Schlame, M., Zhao, M., Gu, Z., Klingenberg, M., Pfanner, N., and Greenberg, M.L. (2000). Absence of cardiolipin in the crd1 null mutant results in decreased mitochondrial membrane potential and reduced mitochondrial function. J. Biol. Chem. *275*, 22387–22394.

Jin, S.M., and Youle, R.J. (2013). The accumulation of misfolded proteins in the mitochondrial matrix is sensed by PINK1 to induce PARK2/Parkin-mediated mitophagy of polarized mitochondria. Autophagy *9*, 1750–1757.

Johnson, L.V., Walsh, M.L., Bockus, B.J., and Chen, L.B. (1981). Monitoring of relative mitochondrial membrane potential in living cells by fluorescence microscopy. J. Cell Biol. *88*, 526–535.

Jovaisaite, V., Mouchiroud, L., and Auwerx, J. (2014). The mitochondrial unfolded protein response, a conserved stress response pathway with implications in health and disease. J. Exp. Biol. *217*, 137–143.

Kamath, R.S., and Ahringer, J. (2003). Genome-wide RNAi screening in *Caenorhabditis elegans*. Methods *30*, 313–321.

Köhler, F., Müller-Rischart, A.K., Conradt, B., and Rolland, S.G. (2015). The loss of LRPPRC function induces the mitochondrial unfolded protein response. Aging (Albany N.Y.) 7, 701–717.

Liu, Y., Samuel, B.S., Breen, P.C., and Ruvkun, G. (2014). Caenorhabditis elegans pathways that surveil and defend mitochondria. Nature 508, 406–410.

Loew, L.M., Tuft, R.A., Carrington, W., and Fay, F.S. (1993). Imaging in five dimensions: time-dependent membrane potentials in individual mitochondria. Biophys. J. 65, 2396–2407.

Macario, A.J., Grippo, T.M., and Conway de Macario, E. (2005). Genetic disorders involving molecular-chaperone genes: a perspective. Genet. Med. 7, 3–12.

Martin, J., Mahlke, K., and Pfanner, N. (1991). Role of an energized inner membrane in mitochondrial protein import. Delta psi drives the movement of presequences. J. Biol. Chem. 266, 18051–18057.

Melber, A., and Haynes, C.M. (2018). UPR^{mt} regulation and output: a stress response mediated by mitochondrial-nuclear communication. Cell Res. 28, 281–295.

Nargund, A.M., Pellegrino, M.W., Fiorese, C.J., Baker, B.M., and Haynes, C.M. (2012). Mitochondrial import efficiency of ATFS-1 regulates mitochondrial UPR activation. Science 337, 587–590.

Oliveira, A.N., and Hood, D.A. (2018). Effect of Tim23 knockdown in vivo on mitochondrial protein import and retrograde signaling to the UPR^{mt} in muscle. Am. J. Physiol. Cell Physiol. 315, C516–C526.

Osman, C., Voelker, D.R., and Langer, T. (2011). Making heads or tails of phospholipids in mitochondria. J. Cell Biol. 192, 7–16.

Palikaras, K., Lionaki, E., and Tavernarakis, N. (2015). Coordination of mitophagy and mitochondrial biogenesis during ageing in C. elegans. Nature 521, 525–528.

Pellegrino, M.W., Nargund, A.M., and Haynes, C.M. (2013). Signaling the mitochondrial unfolded protein response. Biochim. Biophys. Acta 1833, 410–416.

Peters, G.-J. (2018). userfriendlyscience: Quantitative analysis made accessible. https://cran.r-project.org/web/packages/userfriendlyscience/index.html.

Pfeiffer, K., Gohil, V., Stuart, R.A., Hunte, C., Brandt, U., Greenberg, M.L., and Schägger, H. (2003). Cardiolipin stabilizes respiratory chain supercomplexes. J. Biol. Chem. 278, 52873–52880.

Pickrell, A.M., and Youle, R.J. (2015). The roles of PINK1, parkin, and mitochondrial fidelity in Parkinson's disease. Neuron 85, 257–273.

Rauthan, M., Ranji, P., Aguilera Pradenas, N., Pitot, C., and Pilon, M. (2013). The mitochondrial unfolded protein response activator ATFS-1 protects cells from inhibition of the mevalonate pathway. Proc. Natl. Acad. Sci. U S A 110, 5981–5986.

Riddle, D.L., Blumenthal, T., Meyer, B.J., and Priess, J.R. (1997). Introduction to C. elegans. In C elegans II, D.L. Riddle, T. Blumenthal, B.J. Meyer, and J.R. Priess, eds. (Cold Spring Harbor Laboratory Press).

RStudio Team (2015). RStudio: Integrated Development for R (RStudio).

Runkel, E.D., Liu, S., Baumeister, R., and Schulze, E. (2013). Surveillance-activated defenses block the ROS-induced mitochondrial unfolded protein response. PLoS Genet. 9, e1003346.

Runkel, E.D., Baumeister, R., and Schulze, E. (2014). Mitochondrial stress: balancing friend and foe. Exp. Gerontol. 56, 194–201.

Sämann, J., Hegermann, J., von Gromoff, E., Eimer, S., Baumeister, R., and Schmidt, E. (2009). Caenorhabditis elegans LRK-1 and PINK-1 act antagonistically in stress response and neurite outgrowth. J. Biol. Chem. 284, 16482–16491.

Sato, Y., Nakajima, S., Shiraga, N., Atsumi, H., Yoshida, S., Koller, T., Gerig, G., and Kikinis, R. (1998). Three-dimensional multi-scale line filter for segmentation and visualization of curvilinear structures in medical images. Med. Image Anal. 2, 143–168.

Schindelin, J. (2012). Fiji: an open-source platform for biological-image analysis. Nat. Methods 9, 676–682.

Shaye, D.D., and Greenwald, I. (2011). OrthoList: a compendium of C. elegans genes with human orthologs. PLoS ONE 6, e20085.

Springer, W., Hoppe, T., Schmidt, E., and Baumeister, R. (2005). A Caenorhabditis elegans Parkin mutant with altered solubility couples alpha-synuclein aggregation to proteotoxic stress. Hum. Mol. Genet. 14, 3407–3423.

Sternberg, S.R. (1983). Biomedical image processing. Computer 16, 22–34.

Stiernagle, T. (2006). Maintenance of C. elegans. In WormBook: The Online Review of C elegans Biology. http://www.wormbook.org/chapters/www_strainmaintain/strainmaintain.html.

Vabulas, R.M., Raychaudhuri, S., Hayer-Hartl, M., and Hartl, F.U. (2010). Protein folding in the cytoplasm and the heat shock response. Cold Spring Harb. Perspect. Biol. 2, a004390.

Wiedemann, N., and Pfanner, N. (2017). Mitochondrial machineries for protein import and assembly. Annu. Rev. Biochem. 86, 685–714.

Wiedemann, N., Truscott, K.N., Pfannschmidt, S., Guiard, B., Meisinger, C., and Pfanner, N. (2004). Biogenesis of the protein import channel Tom40 of the mitochondrial outer membrane: intermembrane space components are involved in an early stage of the assembly pathway. J. Biol. Chem. 279, 18188–18194.

Xu, S., and Chisholm, A.D. (2014). C. elegans epidermal wounding induces a mitochondrial ROS burst that promotes wound repair. Dev. Cell 31, 48–60.

Yano, M. (2017). ABCB10 depletion reduces unfolded protein response in mitochondria. Biochem. Biophys. Res. Commun. 486, 465–469.

Yoneda, T., Benedetti, C., Urano, F., Clark, S.G., Harding, H.P., and Ron, D. (2004). Compartment-specific perturbation of protein handling activates genes encoding mitochondrial chaperones. J. Cell Sci. 117, 4055–4066.

Zhao, Q., Wang, J., Levichkin, I.V., Stasinopoulos, S., Ryan, M.T., and Hoogenraad, N.J. (2002). A mitochondrial specific stress response in mammalian cells. EMBO J. 21, 4411–4419.

Zubovych, I.O., Straud, S., and Roth, M.G. (2010). Mitochondrial dysfunction confers resistance to multiple drugs in Caenorhabditis elegans. Mol. Biol. Cell 21, 956–969.

STAR★METHODS

KEY RESOURCES TABLE

REAGENT or RESOURCE	SOURCE	IDENTIFIER
Antibodies		
Rabbit anti-HSP-6	Köhler et al., 2015	N/A
Mouse anti-HSP-60	(Hadwiger et al., 2010) available at DHSB	HSP60 s
Rabbit anti-ATFS-1	Gift from C. Haynes (UMass Medical School)	N/A
Mouse anti-Tubulin DM1a	Sigma-Aldrich	Cat # T6199; RRID:AB_477583
Mouse anti-β-actin AC-15	Sigma-Aldrich	Cat # A-1978;RRID:AB_476692
Goat Anti-Mouse IgG (HL)-HRP Conjugate antibody	Biorad	Cat # 1706516;RRID:AB_11125547
Goat Anti-Rabbit IgG (HL)-HRP Conjugate antibody	Biorad	Cat # 1706515;RRID:AB_11125142
Bacterial and Virus Strains		
RNAi clones Ahringer library	Kamath and Ahringer, 2003	N/A
OP50	Caenorhabditis Genetics Center	OP50
HT115	Caenorhabditis Genetics Center	HT115
DH5α	ThermoFischer	Cat # 18265017
Chemicals, Peptides, and Recombinant Proteins		
IPTG	Carl-Roth	Cat # CN08.2
TMRE	ThermoFischer Scientific	Cat # T-669
Amersham ECL Western Blotting Detection Reagent	Sigma-Aldrich	Cat # GERPN2106
Amersham ECL prime Western Blotting Detection Reagent	Sigma-Aldrich	Cat # GERPN2236
Experimental Models: Organisms/Strains		
Wildtype C. elegans strain N2	Caenorhabditis Genetics Center	N2
TK22 (*sdhc-1(kn1) III*)	Caenorhabditis Genetics Center	TK22
DA2249 (*spg-7(ad2249) I*)	Caenorhabditis Genetics Center	DA2249
BR2430 (*pdr-1(lg103) III*)	Gift from R. Baumeister (University of Freiburg)	N/A
MD3399 (*pink-1(tm1779) II*)	This study	N/A
CZ19982 (*mcu-1(ju1154) IV*)	Caenorhabditis Genetics Center	CZ19982
SJ4100 (*zcIs13 V*)	Caenorhabditis Genetics Center	SJ4100
SJ4058 (*zcIs9*)	Caenorhabditis Genetics Center	SJ4058
MD3800 (*mcu-1(ju1154) IV; zcIs13 V*)	This study	N/A
MD4205 (*pink-1(tm1779) II; zcIs13 V*)	This study	N/A
MD4203 (*zcIs13 V*)	This study	N/A
MD4001 (*pdr-1(lg103) III; zcIs13 V*)	This study	N/A
MD4002 (*zcIs13 V*)	This study	N/A
MD4126 (*gcn-2(ok871) II; zcIs13 V*)	This study	N/A
MD4164 (*gcn-2(ok886) II; zcIs13 V*)	This study	N/A
MD4165 (*zcIs13* V)	This study	N/A
MD4284 (*oxTi179 II; unc-119(ed3) III; atfs-1(tm4525) V zcIs9 V*)	This study	N/A
MD4306 (*bcSi78* [*pCFJ350*] II; *unc-119(ed3)* III; *atfs-1 (tm4525) zcIs9* V)	This study	N/A

Continued

REAGENT or RESOURCE	SOURCE	IDENTIFIER
MD4314 (*bcSi80* [*pBC1753*] II; *unc-119*(*ed3*) III; *atfs-1* (*tm4525*) *zcIs9* V)	This study	N/A
MD4323 (*bcSi81* [*pBC1759*] II; *unc-119*(*ed3*) III; *atfs-1* (*tm4525*) *zcIs9* V)	This study	N/A
Oligonucleotides		
Forward primer to amplify *Patfs-1:atfs-1[CDS]:atfs-1 [3′UTR]* from gDNA *atfs-1FSpeI* 5′-ACTAGTTATCCC GATTCAAATCATTG-3′	This study	N/A
Reverse primer to amplify *Patfs-1:atfs-1[CDS]:atfs-1 [3′UTR]* from gDNA *atfs-1RAvrII* 5′-CCTAGGTTACAC AACTGCGTCACG-3′	This study	N/A
Primer for sequencing RNAi clones *L4440 F* 5′-TGGA TAACCGTATTACCGCC-3′	This study	N/A
Recombinant DNA		
pCFJ350 (empty MosSCI vector)	Addgene	Plasmid #34866
pBC1753 (*Patfs-1:atfs-1[CDS with afts-1MTS]: atfs-1[3′UTR]*)	This study	N/A
pBC1759 (*Patfs-1:atfs-1[CDS with su9MTS]: atfs-1[3′UTR]*)	This study	N/A
Software and Algorithms		
Fiji v. 2.0.0-rc-69/1.52i	Schindelin, 2012	https://imagej.net/Fiji/Downloads
Prism v. 6	GraphPad Software	https://www.graphpad.com/scientific-software/prism/
MitoProt	Claros and Vincens, 1996	https://ihg.gsf.de/ihg/mitoprot.html
Leica Application Suite v. 3.2.0.9652	Leica Microsystems	https://www.leica-microsystems.com/products/microscope-software/p/leica-application-suite/
Metamorph v. 7.1.0.0.	Molecular Device Corporation	https://www.moleculardevices.com/
David Database v. 6.8	Huang et al., 2009	https://david.ncifcrf.gov
Image Lab v. 5.2.1. build 11	Bio-Rad	http://www.bio-rad.com/de-de/product/image-lab-software
R Studio v. 1.1.423 with "userfriendlyscience" package	RStudio Team, 2015; Peters, 2018	https://www.rstudio.com

LEAD CONTACT AND MATERIALS AVAILABILITY

Further information and requests for resources and reagents should be directed to and will be fulfilled by the Lead Contact, Barbara Conradt (b.conradt@ucl.ac.uk).

All *C. elegans* strains and plasmids generated in this study are freely available upon request to the Lead Contact, Barbara Conradt (b.conradt@ucl.ac.uk).

EXPERIMENTAL MODEL AND SUBJECT DETAILS

C. elegans strains and culture conditions

C. elegans strains were cultured as previously described (Brenner, 1974). Bristol N2 was used as the wild-type strain. The screen was performed using the strain SJ4100, which carries the P$_{hsp-6}$*GFP* transcriptional reporter (Yoneda et al., 2004). Further experiments were performed using the strain SJ4058, which carries the mitochondrial chaperone *hsp-60* transcriptional reporter (P$_{hsp-60}$*GFP*) (Yoneda et al., 2004). Mutations used in this study were described by Riddle et al. (1997) except: (LG I) *spg-7*(*ad2249*) (Zubovych et al., 2010) (LG II) *gcn-2*(*ok871*) and *gcn-2*(*ok886*) (OMRF Knockout Group), *pink-1*(*tm1779*) (National BioResource Project), (LGIII) *pdr-1*(*lg103*) (Springer et al., 2005) and *mev-1*(*kn1*) (Honda et al., 1993), (LGIV) *mcu-1*(*ju1154*) (Xu and Chisholm, 2014) and (LGV) *atfs-1*(*tm4525*) (National BioResource Project).

Transgenic lines generation

To generate the *atfs-1* rescuing construct (*Patfs-1:atfs-1[CDS]:atfs-1[3′UTR]*), we used as a promoter the ∼2.4kb DNA fragment between *ZC376.6*, the gene upstream of *atfs-1*, and the coding sequence of *atfs-1*. As a 3′UTR, we used the ∼300bp DNA fragment downstream of the coding sequence of *atfs-1*, which is described in Wormbase as the 3′UTR of *atfs-1*. *Patfs-1:atfs-1[CDS]:atfs-1 [3′UTR]* was amplified from gDNA using the primer *atfs-1FSpeI* (5′-ACTAGTTATCCCGATTCAAATCATTG-3′) and *atfs-1RAvrII* (5′-CCTAGGTTACACAACTGCGTCACG-3′) and cloned into the MosSCI vector pCFJ350 to generate pBC1753. A second plasmid (pBC1759) was generated, in which the first 24 amino acids of ATFS-1 were replaced with the first 69 amino acids of the subunit 9 of ATP synthase of *Neurospora crassa*. In order to generate stably integrated, single-copy transgenes of these two constructs as well as the control vector, both plasmids as well as the empty pCFJ350 vector were used for MosSCI injection of the strain MD4284 (*oxTi179* II; *unc-119(ed3)* III; *atfs-1(tm4525) zcIs9* [P*hsp-60*GFP] V). To generate the MD4284 strain, we crossed the strain CMH5 (*atfs-1(tm4525) zcIs9* [P*hsp-60*GFP] V) (kind gift from C. Haynes) and EG8079 (*oxTi179* II *unc-119(ed3)* III). To determine the level of the ATFS-1 protein, the different transgenic lines were treated with *tag-208(RNAi)* or *lonp-1(RNAi)* and analyzed by Western using affinity purified rabbit anti-ATFS-1 antibodies (1:5000; generated by Nargund et al. [2012]) and anti-β-actin antibodies (1:2000, Sigma). We also generated a single copy *atfs-1(wt)::GFP* transgene. In contrast to the non-tagged *atfs-1(wt)* transgene, which restores the induction of the P*hsp-60*GFP reporter upon *spg-7(RNAi)* to ∼58% of wild-type level, the *afts-1(wt)::GFP* single copy transgene restores the induction of the P*hsp-60*GFP reporter to only ∼14% of wild-type level. Hence, the presence of GFP appears to negatively affect the ability of ATFS-1 to function as a transcription factor. The name and genotype of all the transgenic lines generated in this study are indicated in Table S2.

METHOD DETAILS

Genome wide RNA interference screen

The screen was performed using the technique of RNAi by feeding using the Ahringer RNAi library (Kamath and Ahringer, 2003).We specifically used the latest updated version of the library which covers more than 90% of the annotated genes of the *C. elegans* genome and is available from Source BioScience (www.lifesciences.sourcebioscience.com).

For the L4 screen, RNAi clones were cultured overnight in 100 μL of LB carbenicillin (100 μg/ml) in a 96 wells plate format on day 1. On day 2, 10 μL of the culture was used to inoculate 24 well lactose RNAi plates (similar to NGM medium (Stiernagle, 2006) with 4g/l bacto-tryptone instead of 2.5g/l of Bacto-Peptone and supplemented with 100 μg/ml Carbenicillin and 0.25% lactose (w/v)) and the plates were incubated at room temperature until the next day. On day 3, a synchronized population of L4 of the SJ4100 strain (P*hsp-6*GFP) was resuspended in MPEG (M9 medium (Stiernagle, 2006) supplemented with 0.1% PEG (w/v)). Two L4 larvae were pipetted in each well of the 24 well plates. The plates were incubated at 20°C for four days and screened for GFP positive progeny. Positive candidates were re-screened in three independent experiments using 24 well 6mM IPTG RNAi plates (NGM medium (Stiernagle, 2006) supplemented with 25 μg/ml Carbenicillin and 6mM IPTG). As indicated in Table S1, the level of induction of UPR^mt was classified from 0 (basal expression of the P*hsp-6*GFP reporter similar to the one observed in *tag-208(RNAi)* animals) to 3 (strong expression of the P*hsp-6*GFP reporter).

For the L1 screen, a sub-library containing the 2000 genes described as essential for embryonic and larval development according to Ahringer and co-workers was generated (Kamath and Ahringer, 2003). RNAi clones were cultured overnight in 100 μL of LB carbenicillin (100 μg/ml) in a 96 well plate format on day 1. On day 2, 10 μL of the culture was used to inoculate 24 well lactose RNAi plates (see above) and the plates were incubated at room temperature until the next day. On day 2, gravid adults of the SJ4100 strain (P*hsp-6*GFP) were bleached as previously described (Stiernagle, 2006). The embryos were incubated overnight in M9 medium in order to produce a synchronized population of L1 larvae the next morning. On day 3, 50 synchronized L1 larvae were inoculated onto each well of the 24 wells Lactose RNAi plates. The plates were incubated at 20°C for three days and screened for GFP positive animals. Positive candidates were re-screened in three independent experiments using 24 wells 6mM IPTG RNAi plates (see above).

Bioinformatic analysis

For prediction of the mitochondrial targeting sequence and its charge, we used the Mitoprot software ((Claros and Vincens, 1996); https://ihg.gsf.de/ihg/mitoprot.html). For the functional annotations and clustering we used the DAVID database v. 6.8 (Huang et al., 2009). The list of candidates was used as an input and was ran against the *C. elegans* background list for searching of enriched GO categories. The GO-term enrichment is calculated using a modified Fisher's exact test. The so-called EASE score provides a more conservative method to calculate the enrichment of a term, guaranteeing results consistency.

Further analysis of the candidates

RNAi clones were cultured overnight in 2ml of LB carbenicillin (100 μg/ml) at 37°C and 200rpm. The RNAi cultures were adjusted to 0.5OD and 50 μL was used to seed 30mm RNAi plates containing 6mM IPTG (see above). The plates were incubated at 20°C in the dark. [In the case of double RNAi, each RNAi culture was diluted 1:3 with *atfs-1(RNAi)* or *tag-208(RNAi)* bacteria.] 24 hours later, four L4 larvae of SJ4100 or SJ4058 were inoculated onto the RNAi plates and new RNAi plates were seeded. 24 hours later, the four adults of SJ4100 or SJ4058 were transferred onto new seeded RNAi plates and let to lay eggs for 4 hours at 20°C. The adults were then removed from the plates and the plates were further incubated for 4 days at 20°C (For the rescue experiments, the plates

were incubated for 5 days at 20°C). For each RNAi condition, ~10 animals were imaged using a Leica GFP dissecting microscope (M205 FA) and the software Leica Application Suite (3.2.0.9652). We used Fiji-implemented macro using the IJ1 Macro language to automate the intensity measurement within defined areas of 2-dimensional images using ImageJ. An automated threshold using the Triangle method was applied to the brightfield microscopy image, in order to generate a binary mask (The Triangle method was selected among the 16 available auto threshold methods of ImageJ as it provided the best results). The mask was then inverted and the Particle Analyzer of ImageJ was used to remove noise by setting a minimum size (10 pixels) for objects to be included in the mask. After removing manually any remaining unwanted objects, the mask was applied to the corresponding fluorescence microscopy image and mean fluorescence intensity was measured. The mean fluorescence intensity outside the mask was defined as the background. The script ("Worm_SignalQuantification.ijm") used for the analysis can be found in Data S1.

Analysis of HSP-6 and HSP-60 protein levels

Two L4 larvae of N2 were inoculated on *tag-208(RNAi)*, *fum-1(RNAi)* or *sdhc-1(RNAi)* plates and the plates were incubated for 5 days at 20°C. Mixed-stage populations of worms were harvested in 1ml MPEG, washed 3 times with 1ml MPEG and resuspended in 1 volume of Laemmli buffer 2x. The samples were analyzed by SDS-PAGE and Western using a monoclonal anti-Tubulin (1:10000; Sigma), a polyclonal anti-HSP-6 (1:10000; (Köhler et al., 2015)) and a monoclonal anti-HSP-60 (1:2000; generated by Hadwiger et al. (2010) and available at DHSB). As secondary antibodies, we used horseradish peroxidase conjugated goat anti-mouse antibodies (BioRad #1706516) at 1:10000 for the anti-Tubulin and at 1:7500 for the anti-HSP-60. For the anti-HSP-6, we used a horseradish peroxidase conjugated goat anti-rabbit (BioRad #1706515) at 1:10000. Western was developed using ECL (Amersham #RPN2106) and images were quantified using the ChemiDoc XRS+ System (Bio-Rad).

TMRE staining and quantification

L2/L3 larvae were inoculated on NGM plates (Stiernagle, 2006) supplemented with 0.1 μM Tetramethylrhodamine, Ethyl Ester (TMRE) with a small inoculum of OP50 *E. coli* bacteria. After an incubation over-night at 20°C, L4 larvae were analyzed by fluorescence microscopy using a microscope equipped with a 63 × 1.4 NA oil lens (Axioskop 2; Carl Zeiss, Inc.) and a charge-coupled device camera (1300; Micromax). The acquisition was performed with 100ms exposure using the software Metamorph (Molecular Device Corporation; v. 7.1.0.0). For the RNAi experiments, L4 larvae were inoculated onto 6mM IPTG RNAi plates as indicated above. After 2 days, L2/L3 larvae of the F1 generation were inoculated on TMRE plates and analyzed the next day as indicated above. We used Fiji-implemented macro using the IJ1 Macro language to segment the images. Specifically, we used a background subtraction with the "rolling ball" algorithm with a ball radius of 15 pixels to remove continuous background signal from the image (Sternberg, 1983). This was followed by the application of the Tubeness plugin, which generates a score of how tube-like each point in the image is, by using the eigenvalues of the Hessian matrix to calculate the measure of "tubeness" (Sato et al., 1998). The resulting 32-bit image was converted to 8-bit and an automatic threshold (using the IsoData algorithm) was used to generate a binary mask. The final step involved the removal of any particles that are smaller than 10 pixels in size for they are assumed to be noise. After removing manually any remaining unwanted objects, another macro was used to measure mean fluorescence intensity. Specifically, all objects in the binary mask segmented with the first macro were selected and this selection was restored on the original image, allowing to measure the mean fluorescence intensity within regions that correspond to the binary mask. This binary mask corresponds to the TMRE labeled mitochondria in the image. The mean fluorescence intensity outside the mask was defined as the background and was subtracted from the signal. Since the mean fluorescence intensity corresponds to the sum of the gray values of all the pixels in the selection divided by the number of pixels in the selection, the values indicated in Figures 4C and 4D correspond to fluorescence intensities per area. The scripts ("TMRE Hessian_segmentation.ijm" and "TMRE mean_intensity_measurement.ijm") used for the analysis can be found in Data S1.

QUANTIFICATION AND STATISTICAL ANALYSIS

For Figures 1, 2, 3, 5, S1, S2, and S4, n indicates the number of biological replicates analyzed for a given RNAi (One replicate corresponds to one individual RNAi plate. As indicated in METHOD DETAILS, for each replicate ~10 animals were imaged and the mean fluorescence intensity of these animals was measured). For Figure 4, n indicates the number of animals analyzed for a given genotype or RNAi. For Figure S3, n indicates the number of biological replicates analyzed by Western for a given RNAi. In the quantification of all the Figures, the mean values with the standard deviation are indicated. To perform the statistical analyses, we used the software Graphpad Prism 6 and R Studio Version 1.1.423 (RStudio Team, 2015) with the package "userfriendlyscience" (Peters, 2018).When comparing more than two independent groups, we tested the data for normality using the Kolmogorov-Smirnov test or Shapiro-Wilk test depending on sample size and for equal variance using the Brown-Forsythe test. When the data was normally distributed and showed equal variance, we used one-way ANOVA with Bonferroni's multiple comparison test. In the case of heteroscedasticity, we used a Welch's ANOVA with Games-Howell post hoc test. When the data was not normally distributed, we used a Kruskal-Wallis with Dunn's multiple comparisons test. When only comparing two independent groups, we tested for normality using

the Kolmogorov-Smirnov test or Shapiro-Wilk test depending on sample size and for equal variance using the F-test. We used unpaired two-sample t test when the data was normally distributed and Wilcoxon-Mann-Whitney-test when the data was not normally distributed. For the western-blot analysis (Figure S3), we used a one-sample t test when the data was normally distributed and a Wilcoxon signed rank test when the data was not normally distributed.

DATA AND CODE AVAILABILITY

The published article includes all datasets and code generated or analyzed during this study.